Supporting Information

2D NMR-based metabolomics uncovers interactions between conserved biochemical pathways in the model organism *Caenorhabditis elegans*

Yevgeniy Izrayelit[†,⊥], Steven L. Robinette[‡,⊥], Neelanjan Bose[†], Stephan H. von Reuss[†], and Frank C. Schroeder[†*]

[†] Boyce Thompson Institute and Department of Chemistry and Chemical Biology, Cornell University, Ithaca, New York 14853, United States

[‡] Department of Surgery and Cancer, Imperial College London, London, United Kingdom

[⊥] These authors contributed equally

***Corresponding Author:** schroeder@cornell.edu

CONTENTS

Supporting Methods

Automatic Cross Peak Identification and Integration for mvaDANS. Spectral segments are detected from a representative pseudo-spectrum- here, an average spectrum calculated from the mean along the third dimension of the spectral stack. To identify segments of the pseudo-spectrum corresponding to crosspeak regions, a local noise surface is calculated using the AUTOPSY[1] method (equations 1–4). AUTOPSY calculates a point-wise estimation of underlying noise as follows.

1) $$d_x = \min(\sqrt{\frac{1}{n}\sum_{i=1}^{n}\left(\delta_{xi} - \overline{\delta_x}\right)^2})$$

2) $$d_y = \min(\sqrt{\frac{1}{n}\sum_{i=1}^{n}\left(\delta_{iy} - \overline{\delta_y}\right)^2})$$

3) $$b = \min([d_x, d_y])$$

4) $$p_{xy} = \sqrt{(\sqrt{d_x^{\,2} - b^2})^2 + (\sqrt{d_y^{\,2} - b^2})^2 + b^2}$$

Here, d_x and d_y are noise values for each slice x and y in the direct and indirect dimensions of the 2D NMR spectrum, respectively. The noise value for a given slice δ_x or δ_y is calculated by splitting the slice up into 16 regions of size n=F1/16 for the direct dimension and n=F2/16 for the indirect dimension. The noise for that trace is then the standard deviation of the region with the minimum standard deviation as shown in equations 6 and 7. Each point p in the spectrum is intersected by two slices x and y whose noise values are d_x and d_y. The noise at point p_{xy} is combines the noise in slice *x* with the noise in slice *y* with a baseline noise value *b* as in equations 8 and 9. This method of calculating noise is very well suited to the noise structure of 2D NMR data, which is characterized by vertical noise such as T1 and water noise.

Once the noise surface p_{xy} has been calculated, peaks can be detected by identifying local maxima above a certain multiple of the noise surface. While the exact threshold can vary, values of 5-10 detect the large majority of cross-peaks. A threshold

of 10 was used for the high-concentration *C. elegans* samples used here. Segments are then defined as regions adjacent to detected peaks.

Initial spectral segments are identified as regions within 0.04 ppm of a peak in the ^{1}H dimension of homonuclear spectra. In the case of multiplicity, local maxima are grouped together into a single initial segment. Each segment is then labeled with a unique integer value and iterated minimum and maximum filtering expand these initial segments. Min/max filtering has the effect of growing the segments until they encounter another spectral segment or until they reach a maximum frequency range of approximately 0.2 ppm for ^{1}H. This procedure creates spectral segments with non-rectangular bounds that are bounded by nearby resonances yet avoid close cropping of cross-peak line shapes. These segments are then integrated using a trapezoidal numerical integration.

Pattern Recognition using Spectral Bins. Integration of detected spectral segments transforms the 2D NMR dataset from a three-dimensional stack of full resolution 2D spectra (ω_1, ω_2,N) to a two-dimensional matrix of features (N,P) where P is the number of detected segments. The resulting matrix of bin intensities is then normalized using Probabilistic Quotient Normalization[2] and variance stabilized using univariate scaling. These approaches, sometimes referred to as column-wise and row-wise normalization, are frequently applied in metabolomic data processing to account for dilution between samples or receiver gain differences between spectra and balance the variance of high and low intensity signals. Pattern recognition methods PCA and PLS-DA were then applied directly to the transformed bin matrix. The result of pattern recognition is, for each component in the model, a set of N scores showing the similarity of the samples to each other and a vector of P coefficients (referred to as loadings or predictors) that indicate the contribution of each bin to the separation between the samples.

The matrix of peak integrals was also represented as a log2-fold-change vs. median heatmap. The heatmap was clustered using the UPGMA hierarchical clustering algorithm.[3] Representing the bin matrix as a clustered heatmap allows rapid identification of groups of cross-peaks whose differential levels differentiate experimental classes. Additionally, PLS-DA predictors and PCA loadings were ordered

using the clustered indices of the cross peak regions. This representation displays the features of the data that are identified by pattern recognition.

To interpret the model and identify important metabolites, coefficients are back projected onto the full resolution spectra by using the spectral segments. For all segments in the full resolution matrix, the data points within the segment are replaced with the value of the coefficient from pattern recognition of the bin extracted from that segment to produce a full resolution loadings matrix. For stabilized data, loading coefficients are independent of signal intensity and thus peak shape is not visible. To produce full-resolution back-projected loadings that look like 2D NMR spectra, this matrix is then multiplied point-wise by the standard deviation along the third dimension of the 2D NMR stack. To visualize the loadings, contour lines are defined by the back-projected loadings, and the colors of these lines are defined by the coefficients themselves. While the mvaDANS algorithm was applied to dqfCOSY data processed in magnitude mode to reduce the number of local minima/maxima, regions of interest identified by mvaDANS were cross-referenced with the original phase-sensitive data for greater structural detail. mvaDANS is natively compatible with other ^{1}H-^{1}H NMR experiments, including TOCSY, COSY, and NOESY, and is compatible with only a few changes in parameters to heteronuclear experiments, including ^{1}H-^{13}C HSQC.

Validation and Spectral Interpretation. For analysis of *daf-22* specific crosspeaks, the back projection spectrum is overlaid with the original *daf-22* dqfCOSY spectra, processed in phase-sensitive mode. Spin systems including chemical shift and coupling constant values are obtained via manual interpretation of the original phase-sensitive spectra. Using available databases (Reaxys, Beilstein, Scifinder, HMDB, NMRshiftDB, BMRB), hypotheses about partial structures representing the identified spin systems are developed. Partial fractionation of *daf-22* exo-metabolome was used to generate enriched samples of the identified metabolites for further NMR-spectroscopic analysis via HMQC and HMBC (see Section 1.6 above).

Back projections from PCA analysis were used to identify *daf-22* specific crosspeaks. PLS-DA analysis was used to validate the statistically based separation of

wild-type and *daf-22* metabolomes (Figures S7). Back projections from PLS-DA predictors (Figure S8) largely matched the back projection from PC 1 loadings (Figure S4). Peaks prominently present in dqfCOSY spectra of *E. coli OP*-50 metabolite extract (Figure S9) were excluded from further analysis.

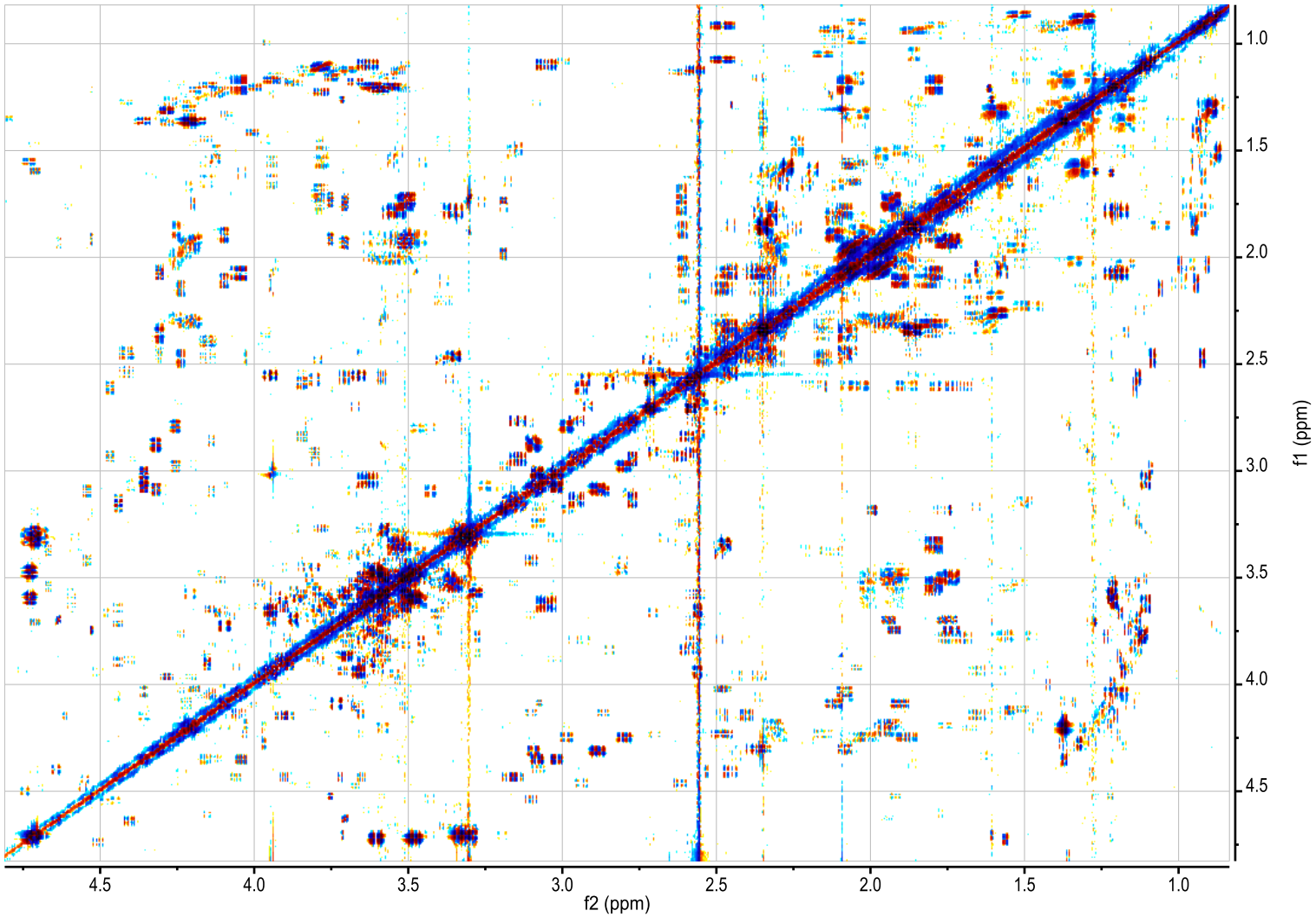

Figure S1. Section (0.85-4.80 ppm) of dqfCOSY of one of four *C. elegans* wild-type exo-metabolome extracts.

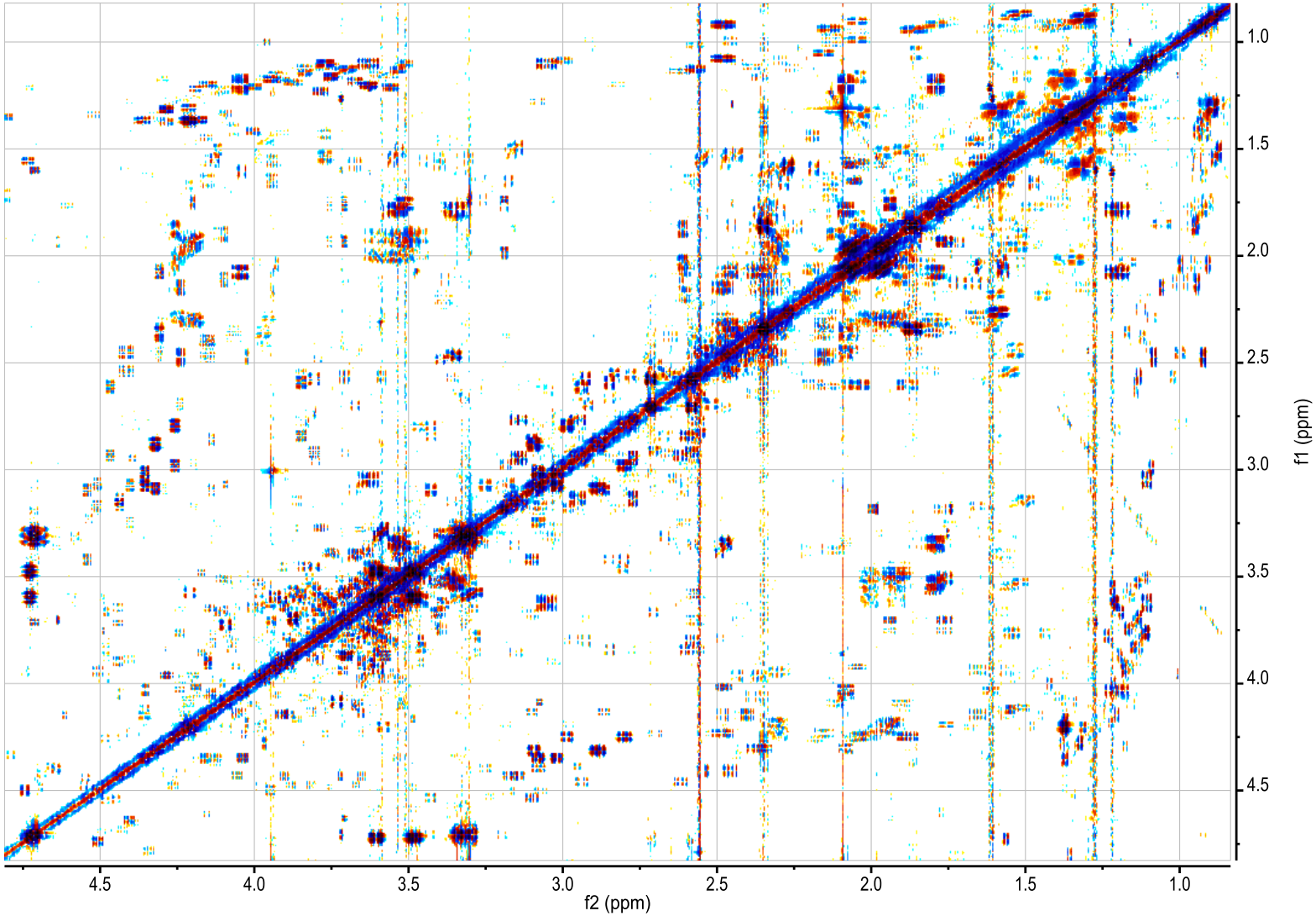

Figure S2. Section (0.85-4.80 ppm) of dqfCOSY of one of four *daf-22(m130)* exo-metabolome extracts.

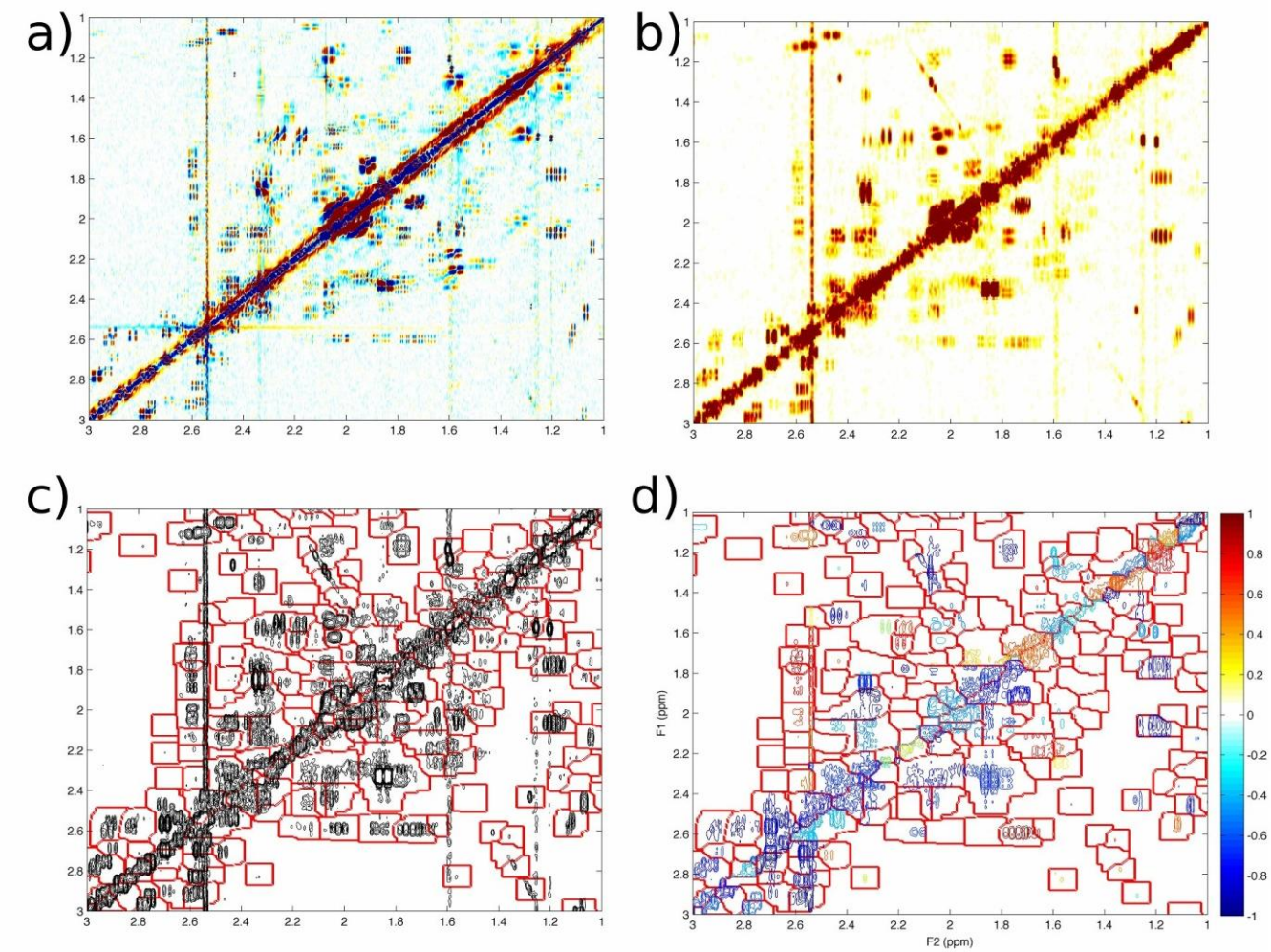

Figure S3. mvaDANS automatically identifies spectral crosspeaks and creates statistically derived pseudo-spectra. a) 1-3 ppm region of phase-sensitive dqfCOSY spectrum of *C. elegans* wild-type metabolome. (b) Same NMR spectrum processed in magnitude mode prior to automatic binning. (c) Contour plot of NMR spectrum from (a) and (b) plotted with boundaries of bin regions identified by mvaDANS. (d) Back-projected pseudo-spectrum derived from Principal Component 1 of the *C. elegans* wild-type/*daf-22* comparison NMR dataset. Crosspeak colors indicate the normalized PC 1 loading coefficient of the region bin.

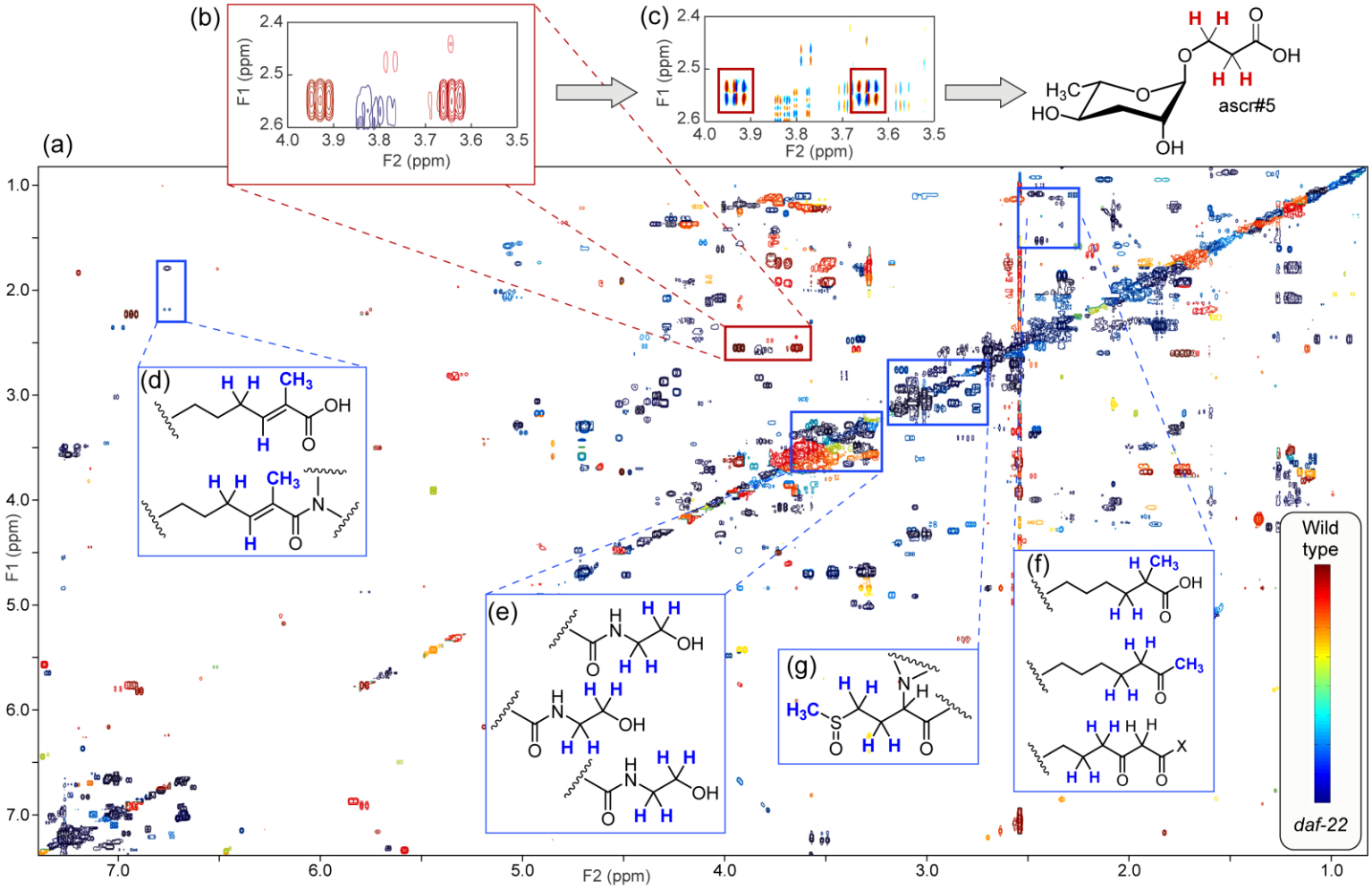

Figure S4. PCA identifies crosspeaks distinguishing wild-type and two *daf-22* mutant alleles. (a) Back-projection of PC 1 loadings onto magnitude mode dqfCOSY spectrum identify crosspeaks increased (red) or decreased (blue) in wild-type spectra relative to mutant spectra. (b, c) Example for mvaDANS work flow and method validation via identification of a known compound. Analysis of crosspeaks in the phase sensitive dqfCOSY-spectrum shown in (c) corresponding to the wild-type specific red crosspeaks in (b) reveals the known ascaroside ascr#5, whose biosynthesis has previously been shown to be *daf-22* dependent. Similarly, most of the other wild-type specific (red) signals in (a) can be assigned to one of the known ascaroside pheromones. Also see Figure S7. (d-f) Partial structures inferred from analysis of *daf-22*-specific crosspeaks that suggest α-methyl branched fatty acids, methyl ketones, and β-keto fatty acid derivatives. (g) Example for not strictly *daf-22* specific metabolite (a putative methionine derivative). This compound is upregulated in *daf-22* mutants but also present in wild-type.

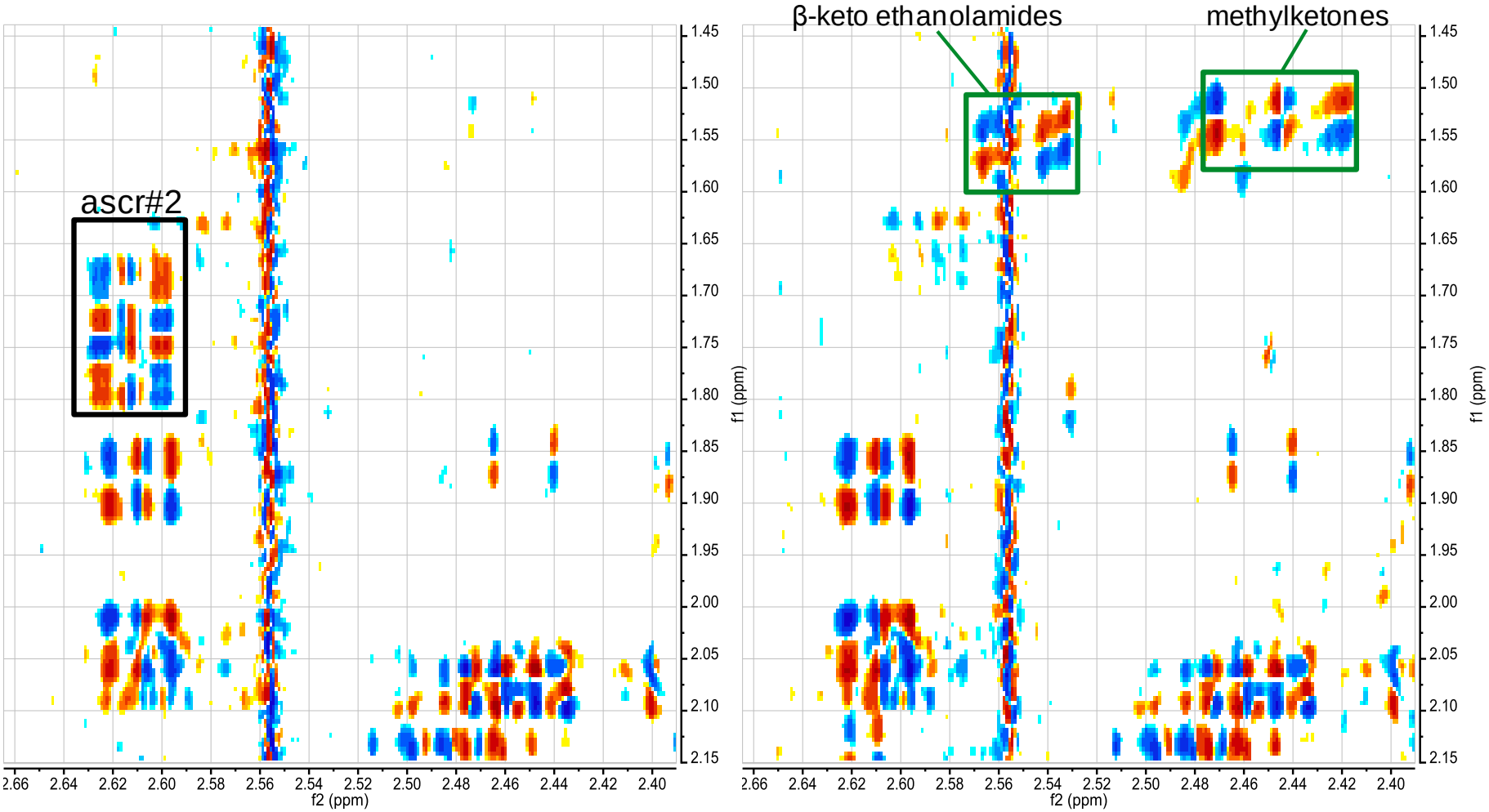

Figure S5. Examples for differential crosspeaks identified by mvaDANS. Left: ascr#2-crosspeaks detected in wild-type spectrum from Figure S5; right: β-keto ethanolamide and methylketone crosspeaks detected in the *daf-22(m130)* spectrum from Figure S3.

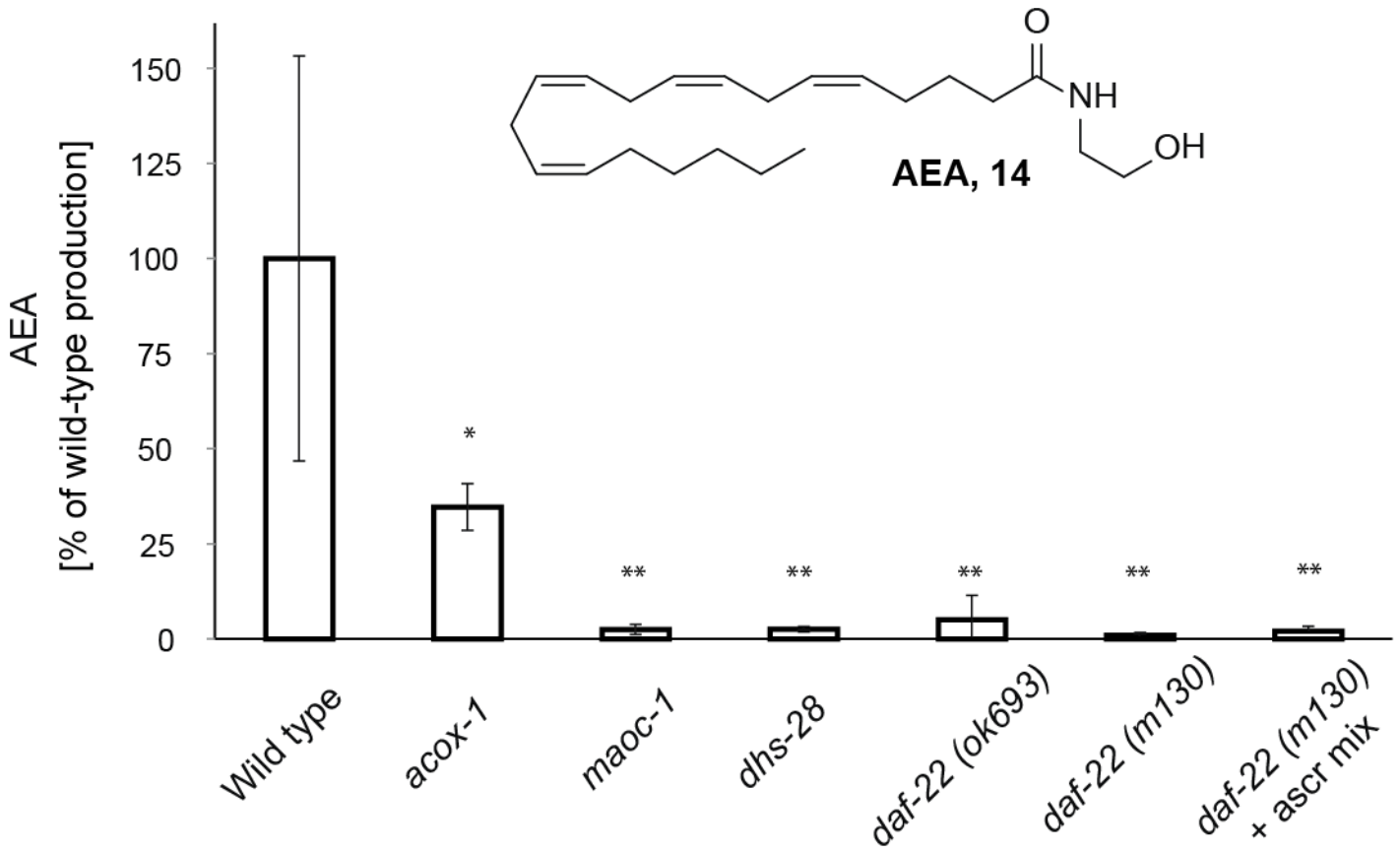

Figure S6. Mutation of *maoc-1*, *dhs-28*, and *daf-22* greatly reduces AEA production, while mutation of *acox-1* slightly decreases AEA production. * P<0.05, ** P<0.01, *** P<0.001.

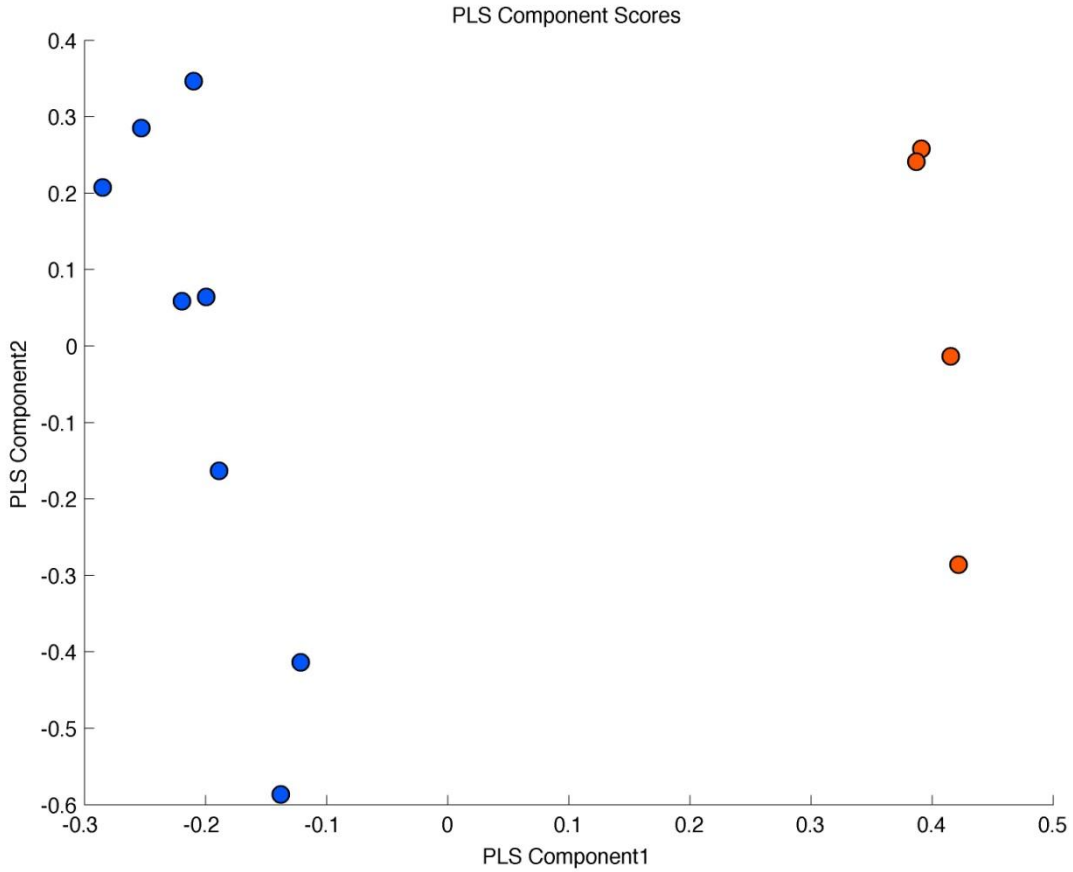

Figure S7. PLS component scores separate 4 wildtype cultures (red dots) from 8 *daf-22* cultures (blue dots).

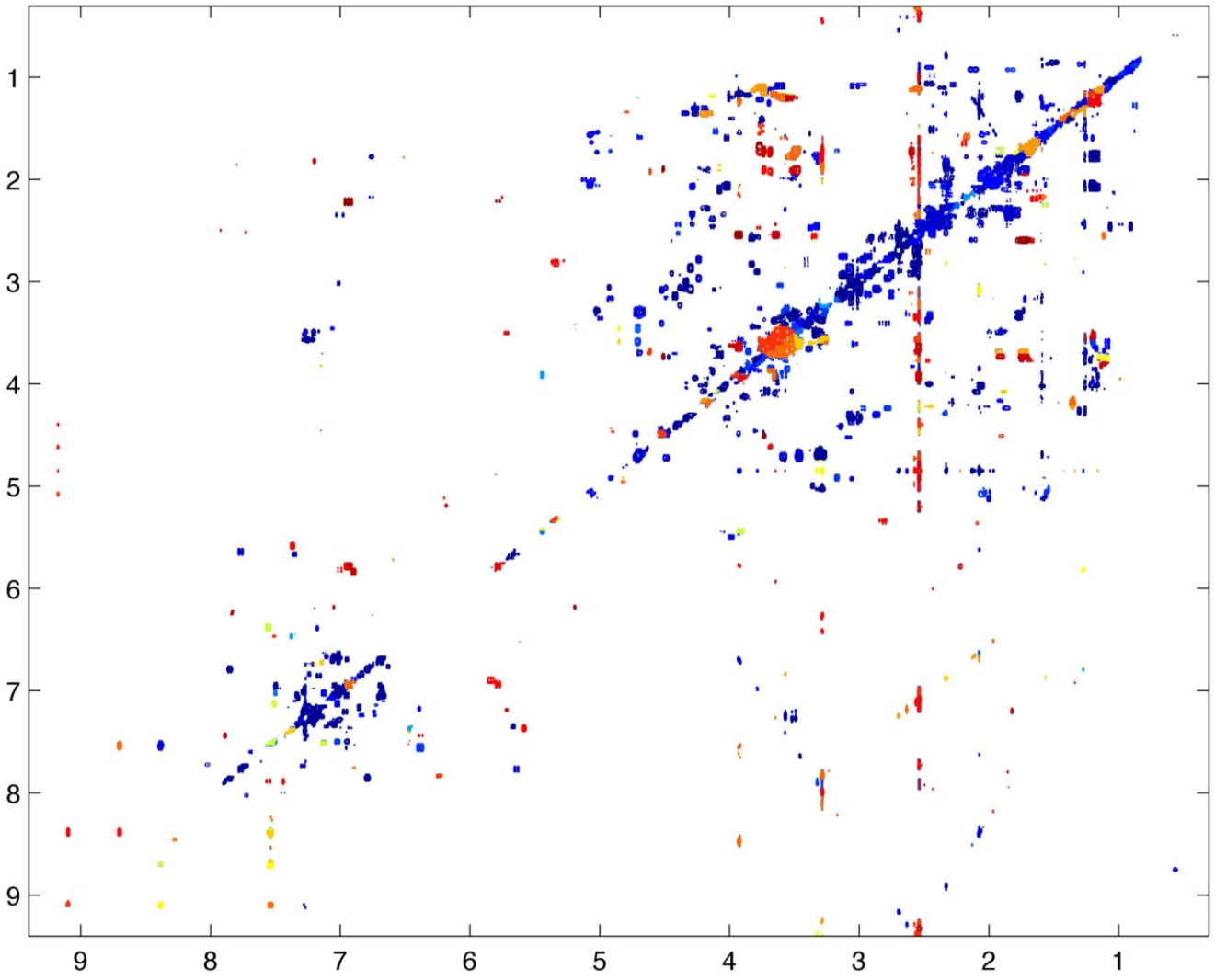

Figure S8. Back projection of PLS-DA predictors from 1 component model with 4x cross validation, largely matching the result from PCA (Figure 3). More significant PLS-DA results would be achieved using a larger number of replicates for wild-type.

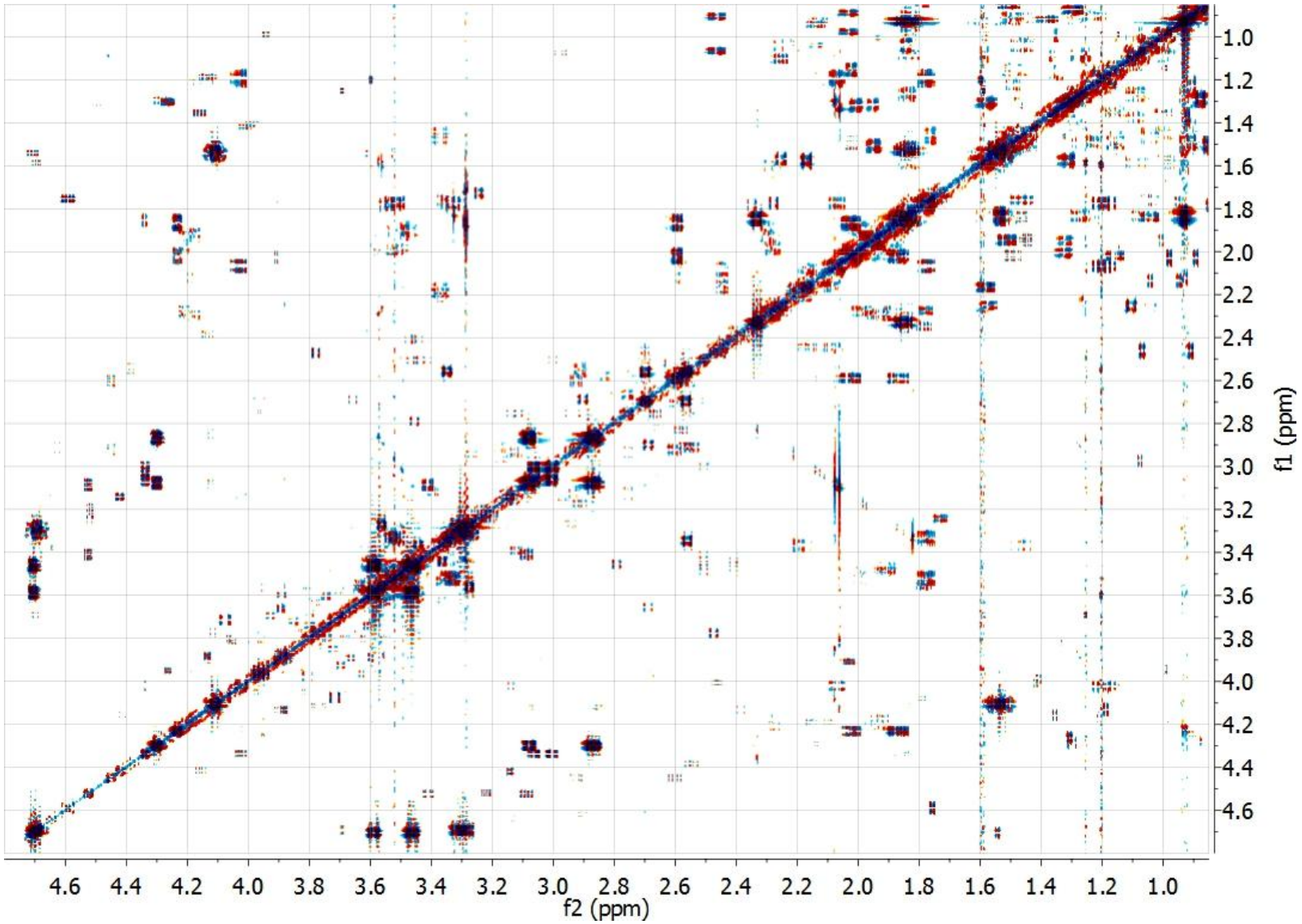

Figure S9. Section (0.85-4.80 ppm) of dqfCOSY of *E. coli* OP50 for exo-metabolome extracts.

Spectroscopic Data of *daf-22*-Upregulated Metabolites

(24*R*)-(3'*R*,5'*R*-Dihydroxy-6'*S*-methyl-(*2H*)-tetrahydropyran-2'-yloxy)-2-methyl-3-oxopentacosanoic acid ethanolamide (7).

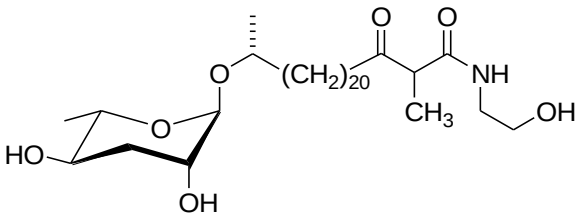

^{1}H NMR ($CDCl_3$, 600 MHz): δ 4.69 (m, 1H, 2'-H); 3.81 (m, 1H, 3'-H); 1.86 (ddd, *J* = 13.5, *J* = 11.0, *J* = 3.1, 1H, 4'-H_{ax}); 2.08 (ddd, *J* = 13.5, *J* = 4.5, *J* = 3.3, 1H, 4'-H_{eq}); 3.60 (ddd, *J* = 11.0, *J* = 9.2, *J* = 4.5, 1H, 5'-H); 3.70 (dq, *J* = 9.2, *J* = 6.3, 1H, 6'-H); 1.27 (d, *J* = 6.3, 3H, 6'-C$\underline{H}_3$); 1.12 (d, *J* = 6.2, 3H, 25-H); 3.79 (m, 1H, 24-H); 1.56 (m, 1H, 23-H); 1.43 (m, 1H, 23-H); 1.30-1.20 (m, 34H, 6-22H); 1.56 (m, 2H, 5-H); 2.55 (td, *J* = 7.3, *J* = 2.3, 2H, 4-H, 3.45 (qd, *J* = 6.5, *J* = 2.3, 1H, 2-H); 1.40 (d, *J* = 6.5, 3H, 2-C$\underline{H}_3$); 3.43 (q, *J* = 5.2, 2H, 1''-H); 3.72 (t, *J* = 5.0, 2H, 2''-H); 6.72 (t, *J* = 5.5, 1H, N-H).

^{13}C NMR ($CDCl_3$, 151 MHz): δ 96.0 (C-2'); 69.4 (C-3'); 35.1 (C-4'); 68.1 (C-5'); 69.7 (C-6'); 17.6 (6'-$\underline{C}H_3$); 18.9 (C-25); 71.7 (C-24); 37.2 (C-23); 28.9-30.5 (C-22 – C-6); 23.3 (C-5); 41.7 (C-4); 210.3 (C-3); 54.0 (C-2); 15.3 (2-$\underline{C}H_3$) 171.1 (C-1); 42.5 (C-1''); 62.3 (C-2'').

HR-MS (ESI$^+$) calculated for $C_{34}H_{65}NO_7Na$ $[M+Na]^+$ 622.4653, observed 622.4728.

(26*R*)-(3'*R*,5'*R*-Dihydroxy-6'*S*-methyl-(*2H*)-tetrahydropyran-2'-yloxy)-3-oxo-heptacosanoic acid ethanolamide (8).

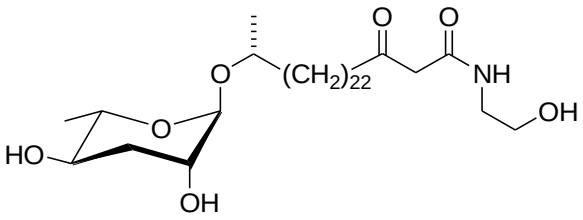

^{1}H NMR ($CDCl_3$, 600 MHz): δ 4.70 (m, 1H, 2'-H); 3.81 (m, 1H, 3'-H); 1.84 (ddd, *J* = 13.5, *J* = 11.0, *J* = 3.1, 1H, 4'-H_{ax}); 2.07 (ddd, *J* = 13.5, *J* = 4.5, *J* = 3.3, 1H, 4'-H_{eq}); 3.61 (ddd, *J* = 11.0, *J* = 9.3, *J* = 4.5, 1H, 5'-H); 3.69 (dq, *J* = 9.3, *J* = 6.2, 1H, 6'-H); 1.27 (d, *J* = 6.3, 3H, 6'-C$\underline{H}_3$); 1.12 (d, *J* = 6.2, 3H, 27-H); 3.79 (m, 1H, 26-H); 1.56 (m, 1H, 25-H); 1.42 (m, 1H, 25-H); 1.30-1.20 (m, 38H, 6-24H);1.57 (m, 2H, 5-H), 2.53 (t, *J* = 7.5, 2H, 4-H), (3.43, s, 2H, 2-H), 3.46 (q, *J* = 5.2, 2H, 1''-H); 3.74 (t, *J* = 5.0, 2H, 2''-H); 7.42 (t, *J* = 5.5, 1H, N-H).

^{13}C NMR ($CDCl_3$, 151 MHz): δ 96.1 (C-2'); 69.4 (C-3'); 35.1 (C-4'); 68.1 (C-5'); 69.7 (C-6'); 17.6 (6'-$\underline{C}H_3$); 18.9 (C-27); 71.7 (C-26); 37.2 (C-25); 28.9-30.5 (C-24 – C-6); 23.3 (C-5); 44.0 (C-4); 207.4 (C-3); 48.4 (C-2); 167.0 (C-1); 42.6 (C-1''); 62.3 (C-2'').

HR-MS (ESI$^+$) calculated for $C_{35}H_{67}NO_7Na$ $[M+Na]^+$ 636.4810, observed 636.4851.

(24*R*)-(3'*R*,5'*R*-Dihydroxy-6'*S*-methyl-(*2H*)-tetrahydropyran-2'-yloxy)-2-methyl-2*E*-pentacosenoic acid ethanolamide (9).

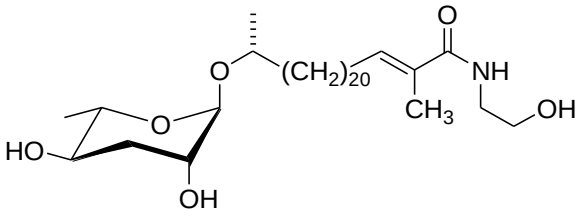

^{1}H NMR ($CDCl_3$, 600 MHz): δ 4.70 (m, 1H, 2'-H); 3.81 (m, 1H, 3'-H); 1.84 (ddd, *J* = 13.5, *J* = 11.0, *J* = 3.1, 1H, 4'-H_{ax}); 2.07 (ddd, *J* = 13.5, *J* = 4.5, *J* = 3.3, 1H, 4'-H_{eq}); 3.61 (ddd, *J* = 11.0, *J* = 9.4, *J* = 4.5, 1H, 5'-H); 3.70 (dq, *J* = 9.4, *J* = 6.2, 1H, 6'-H); 1.28 (d, *J* = 6.2,

3H, 6'-C<u>H</u>$_3$); 1.12 (d, *J* = 6.2, 3H, 25-H); 3.79 (m, 1H, 24-H); 1.56 (m, 1H, 23-H); 1.42 (m, 1H, 23-H); 1.34-1.20 (m, 34H, 6-22H); 1.41 (m, 2H, 5-H); 2.14 (q, *J* ≈ 7.2, 2H, 4-H); 6.41 (tq, *J* = 7.2, *J* = 1.2, 1H, 3-H); 1.86 (m, 3H, 2-C<u>H</u>$_3$); 3.50 (q, *J* = 5.2, 2H, 1''-H); 3.77 (t, *J* = 5.0, 2H, 2''-H); 6.15 (t, *J* = 5.5, 1H, N-H).

^{13}C NMR ($CDCl_3$, 151 MHz): δ 96.1 (C-2'); 69.4 (C-3'); 35.1 (C-4'); 68.1 (C-5'); 69.7 (C-5'); 17.6 (6'-<u>C</u>H$_3$); 18.9 (C-25); 71.7 (C-24); 37.2 (C-23); 28.9-30.5 (C-22 – C-5); 28.4 (C-4); 137.3 (C-3); 129.9 (C-2); 12.6 (2-<u>C</u>H$_3$); 170.7 (C-1); 42.8 (C-1''); 62.9 (C-2'').

HR-MS (ESI$^+$) calculated for $C_{34}H_{65}NO_7Na$ $[M+Na]^+$ 622.4653, observed 622.4728.

(24*R*)-(3'*R*,5'*R*-Dihydroxy-6'*S*-methyl-(*2H*)-tetrahydropyran-2'-yloxy)-2-methyl-2*E*-pentacosenoic acid (10).

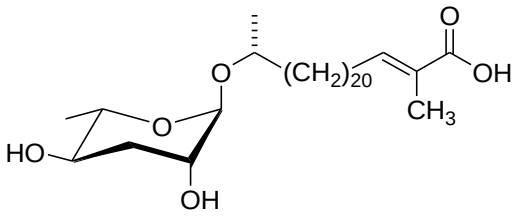

^{1}H NMR ($CDCl_3$, 600 MHz): δ 4.71 (m, 1H, 2'-H); 3.81 (m, 1H, 3'-H); 1.84 (ddd, *J* = 13.5, *J* = 11.0, *J* = 3.1, 1H, 4'-H$_{ax}$); 2.07 (ddd, *J* = 13.5, *J* = 4.5, *J* = 3.3, 1H, 4'-H$_{eq}$); 3.61 (ddd, *J* = 11.0, *J* = 9.4, *J* = 4.5, 1H, 5'-H); 3.70 (dq, *J* = 9.4, *J* = 6.2, 1H, 6'-H); 1.27 (d, *J* = 6.2, 3H, 6'-C<u>H</u>$_3$); 1.12 (d, *J* = 6.2, 3H, 25-H); 3.79 (m, 1H, 24-H); 1.56 (m, 1H, 23-H); 1.42 (m, 1H, 23-H); 1.34-1.20 (m, 34H, 6-22H); 1.45 (m, 2H, 5-H); 2.18 (q, *J* ≈ 7, 2H, 4-H); 6.87 (tq, *J* = 7.2, *J* = 1.4, 1H, 3-H); 1.82 (m, 3H, 2-C<u>H</u>$_3$).

^{13}C NMR ($CDCl_3$, 151 MHz): δ 96.2 (C-2'); 69.4 (C-3'); 35.1 (C-4'); 68.1 (C-5'); 69.7 (C-6'); 17.6 (6'-<u>C</u>H$_3$); 18.9 (C-25); 71.7 (C-24); 37.2 (C-23); 29-30.5 (C-22 – C-5); 28.5 (C-4); 145.0 (C-3); 126.6 (C-2); 12.2 (CH_3-C2); 170.5 (C-1).

HR-MS (ESI$^+$): calculated for $C_{32}H_{60}NO_6Na$ $[M+Na]^+$ 563.4282, observed 563.4283.

(24*R*)-(3'*R*,5'*R*-Dihydroxy-6'*S*-methyl-(*2H*)-tetrahydropyran-2'-yloxy)-2-methyl-pentacosanoic acid (11).

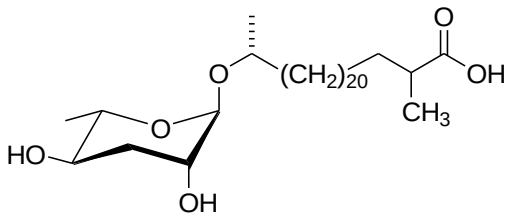

^{1}H NMR ($CDCl_3$, 600 MHz): δ 4.71 (m, 1H, 2'-H); 3.81 (m, 1H, 3'-H); 1.84 (ddd, *J* = 13.5, *J* = 11.0, *J* = 3.1, 1H, 4'-H_{ax}); 2.07 (ddd, *J* = 13.5, *J* = 4.5, *J* = 3.3, 1H, 4'-H_{eq}); 3.60 (ddd, *J* = 11.0, *J* = 9.4, *J* = 4.5, 1H, 5'-H); 3.70 (dq, *J* = 9.4, *J* = 6.3, 1H, 6'-H); 1.27 (d, *J* = 6.3, 3H, 6'-C$\underline{H}_3$); 1.12 (d, *J* = 6.2, 3H, 25-H); 3.79 (m, 1H, 24-H); 1.56 (m, 1H, 23-H); 1.42 (m, 1H, 23-H); 1.35-1.20 (m, 38H, 4-22H); 1.67 (m, 1H, 3-H); 1.42 (m, 1H, 3-H); 2.46 (sext., *J* ≈ 7, 1H, 2-H); 1.17 (d, *J* = 6.8, 3H, 2-CH_3).

^{13}C NMR ($CDCl_3$, 151 MHz): δ 96.2 (C-2'); 69.4 (C-3'); 35.1 (C-4'); 68.1 (C-5'); 69.7 (C-6'); 17.6 (6'-$\underline{C}H_3$); 18.9 (C-25); 71.7 (C-24); 37.2 (C-23); 29.0-30.5 (C-22 – C-4); 28.5 (C-4); 33.8 (C-3); 39.2 (C-2); 17.0 (2-$\underline{C}H_3$); 179.5 (C-1).

HR-MS (ESI$^+$): calculated for $C_{32}H_{60}NO_6Na$ $[M+Na]^+$ 563.4282, observed 563.4283.

(23*R*)-(3'*R*,5'*R*-Dihydroxy-6'*S*-methyl-(*2H*)-tetrahydropyran-2'-yloxy)-tetracosan-2-one (12).

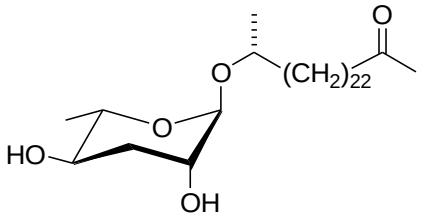

^{1}H NMR ($CDCl_3$, 600 MHz): δ 4.70 (m, 1H, 2'-H); 3.81 (m, 1H, 3'-H); 1.84 (ddd, *J* = 13.5, *J* = 11.0, *J* = 3.1, 1H, 4'-H_{ax}); 2.07 (ddd, *J* = 13.5, *J* = 4.5, *J* = 3.3, 1H, 4'-H_{eq}); 3.59 (ddd, *J* = 11.0, *J* = 9.2, *J* = 4.5, 1H, 5'-H); 3.69 (dq, *J* = 9.2, *J* = 6.2, 1H, 6'-H); 1.27 (d, *J* = 6.2, 3H, 6'-C$\underline{H}_3$); 1.12 (d, *J* = 6.2, 3H, 26-H); 3.79 (m, 1H, 25-H); 1.56 (m, 1H, 24-H); 1.42

(m, 1H, 24-H); 1.35-1.20 (m, 38H, 5-23H); 1.56 (m, 2H, 4-H); 2.41 (t, *J* = 7.5, 2H, 3-H); 2.13 (s, 3H, 1-H).

^{13}C NMR ($CDCl_3$, 151 MHz): δ 96.2 (C-2'); 69.4 (C-3'); 35.1 (C-4'); 68.1 (C-5'); 69.7 (C-6'); 17.6 (6'-$\underline{C}H_3$); 18.9 (C-24); 71.7 (C-23); 37.2 (C-22); 29.0-30.5 (C-21 – C-5); 23.9 (C-4); 43.8 (C-3); 209.6 (C-2); 29.9 (C-1).

HR-MS (ESI$^+$): calculated for $C_{32}H_{62}O_5Na$ $[M+Na]^+$ 549.4495, observed 549.4501.

Table S1. HPLC/HR-MS (ESI$^+$) data of (ω-1)-ascarosyl-2-oxoalkanes in *daf-22* mutants.

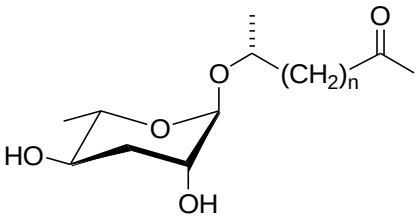

Side chain length (n)	Molecular formula	Molecular weight [amu]	*m/z* $[M+Na]^+$ calculated	*m/z* $[M-Na]^+$ observed	Retention time [min]
18	$C_{28}H_{54}O_5$	470.3971	493.3869	493.3869	6.55
19	$C_{29}H_{56}O_5$	484.4128	507.4025	507.4024	7.33
20	$C_{30}H_{58}O_5$	498.4284	521.4182	521.4178	8.39
21	$C_{31}H_{60}O_5$	512.4441	535.4338	535.4346	9.52
22	$C_{32}H_{62}O_5$	526.4597	549.4495	549.4501	11.14
23	$C_{33}H_{64}O_5$	540.4754	563.4651	563.4650	12.95
24	$C_{34}H_{66}O_5$	554.491	577.4808	577.4807	15.06
25	$C_{35}H_{68}O_5$	568.5067	591.4964	591.4967	17.50
26	$C_{36}H_{70}O_5$	582.5223	605.5121	605.5116	20.55

Supporting References

(1) Koradi, R. (1998) Automated peak picking and peak integration in macromolecular NMR spectra using AUTOPSY, *J. Magn. Reson. 135,* 288–297.

(2) Dieterle, F., Ross, A., Schlotterbeck, G., and Senn, H. (2006) Probabilistic quotient normalization as robust method to account for dilution of complex biological mixtures. Application in 1H NMR metabonomics, *Anal. Chem. 78*, 4281–4290.

(3) Gordon, A. D. (1987) A review of hierarchical-classification, *J. R. Statist. Soc. 150*, 119–137.